Rend. Sem. Mat. Univ. Politec. Torino
Vol. 72, 1–2 (2014), 17 – 36

D. Flynn[1]

A SURVEY OF HYSTERESIS MODELS OF MAMMALIAN LUNGS

Abstract. In this paper, a survey of mathematical models accounting for the pressure-volume relationship with and without hysteresis in mammalian lungs is given. It is shown that a model with a Preisach operator with no additional parameters, based on Venegas' non-hysteretic model, could capture most of the behaviour of observed data. However, the model does not capture the full sigmoidal character of the inflation loop and needs to be further extended.

1. Introduction.

The mammalian lung is a complex organ necessary for respiration. It consists of an inverted tree-like structure shown in Figure 1, which starts at the wind-pipe, branches into two bronchial tubes, which in turn branch into thinner tubes called bronchioles. These bronchioles finally terminate at the alveoli - the tiny air sacs which perform gas exchange with the blood.

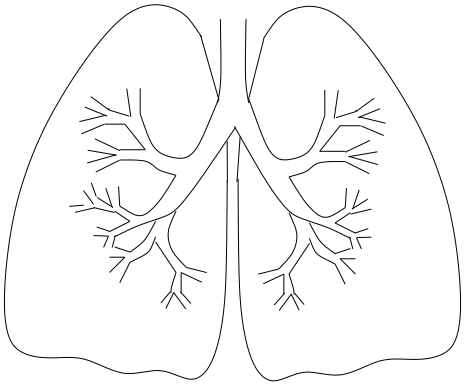

Figure 1: Tree-like structure of the mammalian lungs.

Knowledge of the static mechanical properties of the lung is the basis for understanding the distribution of ventilation, the work of breathing and other parameters of pulmonary function [30]. The static mechanical properties are reflected in the pressure-volume relationship, which is represented by a sigmoidal shaped curve as shown in Figure 2, where the input is the pressure and the output is the volume. This relationship becomes more complex when the pressure is allowed to change direction, in this

[1]CET, ITAM, Academy of Sciences of the Czech Republic

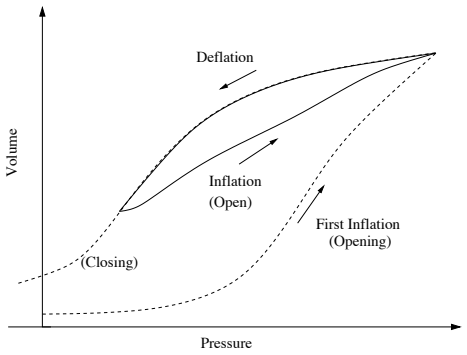

Figure 2: Hysteresis in the pressure-volume relationship of the lungs. Adapted from [10].

case it exhibits hysteresis also shown in Figure 2. In fact it has been found that the qualitative behaviour of Pressure-Volume (P-V) characteristic loops does not vary a whole lot between different species[4].

According to [28], the first measurement of the static pressure-volume relationship of human lungs obtained post mortem, was made by [20] in 1849. However, these measurements were made during inflation only [27]. Measurements for both inflation and deflation of mammalian lungs were first obtained by [11] in 1913, and these measurements exhibited static hysteresis [27].

Early models of the pressure-volume relationship in lungs initially focused on either the inhalation or exhalation limb only [30]. When modelling of hysteresis was initially tackled, the focus was on the rate-dependent aspect. These models were similar to electrical circuits [32], where resistance, impedance, inertance and frequency determined the shape of the P-V loops.

In 1970, Hildebrandt [18] was probably the first to develop a model of rate-independent hysteresis. He found that his linear viscoelastic model accounted for two-thirds of the hysteresis in his data and postulated that the remainder came from a rate-independent plastic strain. He went on to develop a model based on Prandtl bodies, which displayed the qualitative behaviour observed in his data.

In this paper we will briefly outline the medical motivations and background of the lungs and the importance of the knowledge of the P-V relationship. Following this, the mechanisms which are responsible for hysteresis in this relationship will be discussed. In section 5 a brief review of the mathematical modelling efforts will be given. In section 7, we will present mathematical models which we developed and the subsequent results from applying these models to experimental data will also be presented. Finally, conclusions will be drawn in section 8.

2. Medical motivations: mechanical ventilator settings and lung damage

According to [3], P-V curves are used for protective ventilation strategies for patients with lung disease. If the ventilator is set incorrectly, there is a possibility of damage to the patient's lungs, especially those with an underlying condition [2]. Knowledge of these curves when the lungs are in a diseased state such as ARDS (Acute Respiratory Distress Syndrome) [40] is also beneficial. One property that is used quite often is *compliance*, which is a measure of ease of expansion of the lungs. Compliance C is defined as the slope of the P-V relationship i.e. $C = \frac{dV}{dp}$, usually taken at its maximum value [13]. It can change due ageing, inflammation, swelling and denaturalisation of surfactant (which causes increased surface tension) [9].

It has been broadly agreed that a minimum setting should be chosen so as to prevent the alveoli from collapsing, a state known as atelectasis [17, 28, 29]. This minimum setting is known as Positive End-Expiratory Pressure (PEEP) and is set as low as possible that results in acceptable oxygenation [2, 31]. There are various strategies for setting ventilators as outlined by [22] for setting PEEP in patients with ALI (Acute Lung Injury). They introduce a new technique based on the hysteresis of the P-V loops, utilising the vertical distance between the inflation and deflation limbs. It was found that their technique gave the same oxygenation but with lower airway pressures and less over-inflation than other methods. In addition, it was demonstrated during clinical trials by [1, 2], that a ventilator strategy guided by P-V curves resulted in reduced trauma and improved survival compared with conventional strategy without P-V curve guidance [3].

3. Mechanisms of hysteresis

It is understood that hysteresis in the lungs arises from the recruitment and the derecruitment of alveoli and from the surface tension of the surfactant [8, 19] on the interior of alveoli. We will look at these mechanisms in this section.

3.1. Recruitment and derecruitment of alveoli

According to [14], air spaces inflate non-uniformly from the atelectatic (collapsed) state, they inflate in patches and suddenly pop-open, however, they close uniformly during deflation, without collapsing. However, if the surfactant is depleted or chemically altered, the individual alveoli will become unstable during both inflation and deflation.

Suki et al. [35] demonstrated that recruitment of alveoli is the dominant mechanism during *first* inflation. Subsequent inflations are primarily influenced by surface film and connected tissue of the parenchyma. In Cheng et al. [10], derecruitment occurs when the excised lung is deflated below a critical pressure (in rats it was 4 ± 1cm H_2O), at which lung units are sequentially closed. They also noted that additional energy is required to overcome these closed units on inflation and this is reflected in an increase of hysteresis area.

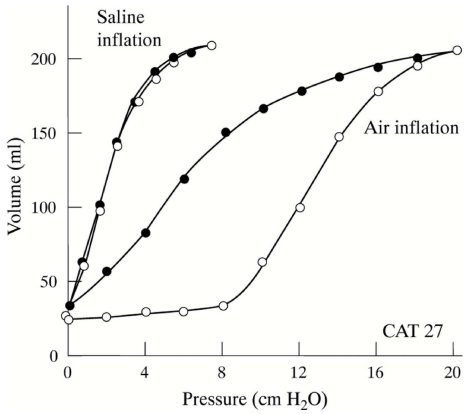

Figure 3: Pressure-volume curves of the respiratory system. The narrow loop on the left was obtained from excised lungs with warm saline solution instead of air. The wider loop on right is formed from inflation (open circles) and deflation (closed circles) of excised lungs. Taken from [21].

In fact the main aim for mechanical ventilators is to keep alveoli from closing, and this is achieved by setting a positive end-expiratory pressure (PEEP) above this critical derecruiting threshold.

The inflation limb of the hysteresis loops generated during first inflation exhibits a plateau as can be seen in Figure 3 (open circles between 0 and 8 cm H_2O), where almost no recruitment occurs. Thereafter, crossing a critical pressure a sudden avalanche [35, 36] of recruitment occurs over a small pressure range. This contrasts significantly with subsequent inflation curves, which contain no such plateau.

3.2. Surface tension of the surfactant

The interior surfaces of alveoli are coated in a thin liquid layer known as the surfactant. It has many properties which facilitate the proper functioning of the lungs and is more than a saline solution, it consists of a liquid layer with a mixture of lipids (90%) and proteins (10%) [8].

Laplace's law, states that pressure p is proportional to the tension T and inversely proportional to the radius R, i.e. $p \propto \frac{T}{R}$, predicts that two unequal alveoli should not remain in equilibrium as shown in Figure 4. The surfactant prevents this collapse [5, 8, 16], as it has the property that its surface tension varies as the area of the surface layer changes, so that T and R in Laplace's equation vary proportionately and p remains equal in all alveoli [8].

According to [15], it was Von Neergaard [38] who in 1929 discovered that the main determinant of hysteresis is air-liquid surface force in alveoli.

In [8], they describe the classic experiment where excised lungs are degassed and P-V curves are measured during a stepwise inflation and deflation manoeuvre,

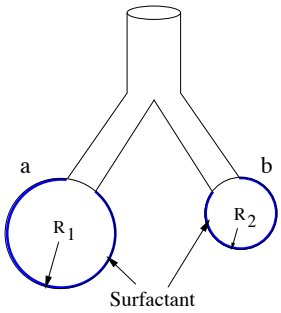

Figure 4: Balancing of alveoli with surfactant.

thus producing the hysteresis loop, shown in Figure 3. This manoeuvre is repeated with warm (37°C) saline solution instead of air, this time it is producing almost no hysteresis, as shown in Figure 3. They make the point, that surface tension disappears as a consequence of the absence of the air-liquid interface.

According to [24], many studies reach the same conclusion, that the air-liquid interface at the alveoli plays an important role in lung mechanics. This is reiterated by [8]. In conclusion, both recruitment and surfactant tension contribute to hysteresis, but dominate at different pressure ranges and pressure histories.

4. Measurements of P-V hysteresis

According to [15], the equations of motion describing the pressure changes of the respiratory system, assuming isotropic expansion, can be written as:

$$p_{AO} = \frac{V}{C} + \dot{V}R + \ddot{V}I - p_{mus}, \tag{1}$$

where the dots denote time-derivatives, p_{AO} is the airway pressure, p_{mus} is the respiratory muscle pressure, $\dot{V}$ is the gas flow, R is the airway resistance and I is the impedance. If the subject is sedated or paralysed then p_{mus} can be eliminated, otherwise the P-V loops may include effects from the respiratory muscle [15]. The term C is the compliance and is one of the main goals in measuring P-V curves. If rate-independence is assumed, the resistance and impedance terms from equation (1) vanish, leaving only the compliance term to be assessed, in fact these *static* P-V curves are often called *compliance curves* [15].

4.1. Static, quasi-static and dynamic hysteresis

In the lung physiology literature [15] the term *static hysteresis* is used instead of *rate-independent hysteresis*. The term *static* denotes that the lung is neither inhaling nor exhaling when measurements are taken. However, it is not advisable to stop the lungs

of a live subject from breathing for too long [15], therefore *quasi-static* measurements are taken.

There are a number of possibilities for measuring quasi-static P-V curves e.g. they can be measured by a stepwise approach, i.e. breathing is paused, and after a relaxation period of about five seconds, measurements are made [15, 37] and the same process is continued. Another approach is to take measurements at a very slow flow rate, at less than 9 L/min, as this minimises the effects of the resistive elements of the respiratory system [15].

The behaviour of P-V curves of the continuously working lung is also of interest to clinicians [15]. In this case *rate-dependent* hysteresis is also observed and is referred to as *dynamic hysteresis* in the literature [15]. However, these curves depend on the frequency, and vary qualitatively from those from the static/quasi-static loops.

5. Mathematical models

Some of the earlier work focused on modelling the P-V curve either during inflation or deflation limb, i.e. without accounting for hysteresis. However, it is possible fit these models to either limb, but it requires a new set of parameters for each inflation or deflation curve. Subsequently hysteresis models were proposed and were based on the idea of either sums or integrals of elements, which had a distribution of threshold values to denote their opening or closure.

5.1. Models without hysteresis

Salazar and Knowles exponential model

One of the earliest expressions used to model the P-V curve during inflation or deflation, was suggested by Salazar and Knowles [33] in 1964. Starting with the assumption that the compliance, $\frac{dV}{dp}$, is proportional to the difference between maximum volume V_M and actual volume V, i.e. $\frac{dV}{dp} = K(V_M - V)$, where K is a constant, and by introducing the half inflation pressure h, such that $e^{-Kh} = \frac{1}{2}$, they came up with the expression

$$V = V_M(1 - e^{-\frac{p\ln 2}{h}}). \tag{2}$$

However, this model did not go far enough to capture the full sigmoidal shape and neither did several subsequent models, which are documented by [30].

Murphy and Engel's sigmoidal model

It was Murphy and Engel [30] who were the first to model the P-V relationship below functional residual capacity (FRC), thus capturing the full sigmoidal shape. Note, however, that the independent variable in their model was volume V instead of p. It

consists of five parameters, as follows:

$$p = \frac{k_1}{V_M - V} + \frac{k_2}{V_m - V} + k_3, \tag{3}$$

where V_M is the upper asymptote, V_m is the lower asymptote and k_1, k_2 are shape parameters and the constant k_3 shifts the curve to the left or to the right [30].

Venegas' four parameter model

An improved model, which was also a sigmoid, was developed by Venegas et al. [39]. Their expression gave an improved fit to P-V data and had one less parameter than [30]. The expression is given by:

$$V = a + \frac{b}{\left(1 + e^{(p-c)/d}\right)}, \tag{4}$$

where V and p are again volume and pressure respectively. Parameter a is the lower asymptote volume, b is the vital capacity or the total change in volume between the lower and upper asymptotes. The parameter c is the pressure at which the inflection point of the sigmoidal curve occurs and which also corresponds to the pressure at the point of highest compliance. Finally parameter d is proportional to the pressure range within which most of the volume changes take place. In addition, [39] showed that the derivative of their expression was a closed form approximation to the normal distribution. They argued that as such the sigmoidal shape of the inflation limb of the P-V curve in ARDS could be reflecting the progressive recruitment of alveolar units with a distribution that follows the normal distribution.

5.2. Models with hysteresis

There have been numerous approaches to the treatment of hysteresis, both for the rate-independent and dependent cases. We will outline these below.

Hildebrandt's Prandtl-bodies model

In the 1970's, Hildebrandt [18] initially developed a linear viscoelastic model to interpret P-V data from cat lungs. He applied pressure in the form of a sinusoid with varying amplitude and varying frequency, in a stepwise fashion to isolated cat lungs. His model was able to account for the stress-relaxation which occurred after each step. It was found that his model was in quantitative agreement with the frequency-dependent compliance of the loops, however, it only accounted for two-thirds of the observed hysteresis. This remaining hysteresis was postulated to be due to the rate-independent plastic strain. He was also able to show that a model based on Prandtl bodies with a distribution of yield points exhibited some of the essential characteristics required to described the dependence of both loop area and amplitude of deformation.

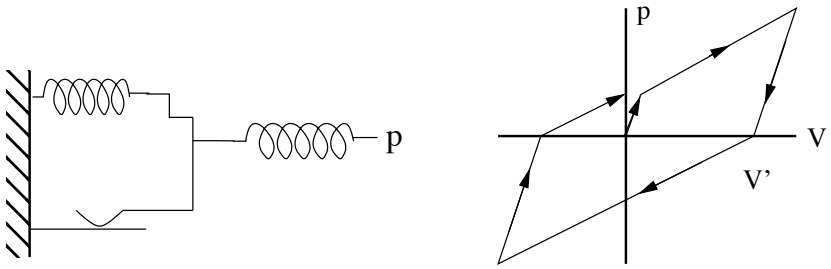

Figure 5: Prandtl body which Hildebrandt used as the smallest element in his static hysteresis model [18].

Starting with the Prandtl body in Figure 5, which is perfectly elastic up to its yield point, after which it undergoes retarded flow. He formulated a model consisting of an arbitrary large number of these units in series, and with a distribution of thresholds representing the strengths of intermolecular linkages. Each unit had a compliance c and the compliance of the system was C. When the pressure $p > p_{T_i}$, i.e. crossed the threshold of the *i-th* unit, stretching of that unit would commence.

The total number of units N would depend on the p. He chose the distribution of thresholds for ease of computation, such that

$$N = \alpha p^{\beta}, \tag{5}$$

where $\alpha > 0, \beta > 0$ were constants. The compliance of the system was then given by:

$$\frac{dV}{dp} = C + cN. \tag{6}$$

From equations (5) and (6), he obtained:

$$V = Cp + rp^{\beta+1}, \tag{7}$$

where $r = \alpha c/(\beta+1)$. This is plotted as curve 1 in Figure 6. To plot curve 2, he translated the coordinate system to point L in Figure 6 and rotated the axis by 180°. To change direction, the force had to be changed by $2p_{T_i}$ and had to be applied, with this force p_1, N_1 elements were moved to the left, where

$$N_1 = \alpha \left(\frac{p_1}{2}\right)^{\beta}, \tag{8}$$

$$\frac{dV_1}{dp_1} = C + cN_1. \tag{9}$$

Similarly, these equations are combined to form:

$$V_1 = Cp + \frac{rp_1^{\beta+1}}{2^{\beta}}, \tag{10}$$

and is plotted as curve 2 in Figure 6. This procedure is repeated to produce further evolution of the system.

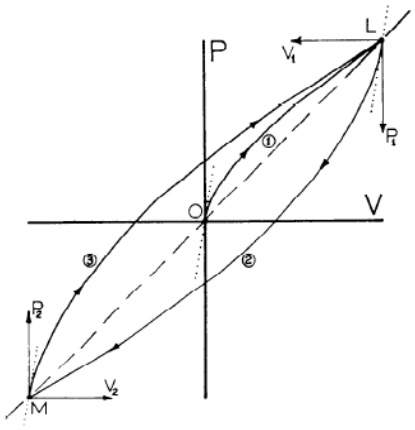

Figure 6: Hildebrandt's [18] plot of the mechanical behaviour of a large number of Prandtl bodies in series.

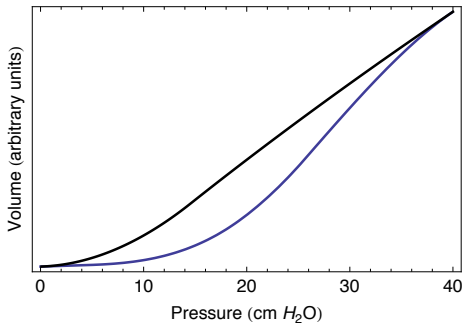

Figure 7: Hickling model: graph of volume vs. pressure, where pressure varied from 0 to 40 cm H_2O for inflation, and back to zero for deflation, completing a full loop.

Hickling's discrete element model

In [17], Hickling models the lungs as a combination of discrete elements, each of which represents an alveolus. These elements are grouped into compartments representing horizontal slices of the lungs, with an increasing gravitational superimposed pressure starting at 0 cm H_2O at the upper compartment and finishing at 15 cm H_2O at the lowermost compartment.

Each element has an associated threshold opening pressure (TOP) or a range of TOPs to simulate alveolar or small airway openings after collapse. While the model was presented as a BASIC programming in [17], it shall be expressed here in a more

concise form to aid with the description:

$$V_{\text{inf}_i} = \sum_{j=1}^{J}\sum_{k=1}^{K}\gamma(p_i - sp_j)\begin{cases}1, & p_i > sp_j + op_k \vee (p_{max} > sp_j + op_k \wedge p_{min} > sp_j),\\ 0, & \text{otherwise},\end{cases}$$

$$V_{\text{def}_i} = \sum_{j=1}^{J}\sum_{k=1}^{K}\gamma(p_i - sp_j)\begin{cases}1, & p_i > sp_j + op_k \vee (p_{max} > sp_i + op_k \wedge p_i > sp_j),\\ 0, & \text{otherwise},\end{cases}$$

where:

$$\begin{aligned} p &= p_{min}, p_{min}+1, \ldots, p_{max},\\ sp &= -0.5, 0, \ldots, 14.5,\\ op &= op_{min}, op_{min}+1, \ldots, op_{max},\\ \gamma &= \frac{K \times V_{unit}}{1 + op_{max} - op_{min}}. \end{aligned}$$

The constant γ is introduced here to factor out common values. The number of units, K is given as 9000 by [17] and their individual volumes are $V_{unit} = 0.0002$. Opening pressures are given by op and range from op_{min} to op_{max}. Each lung compartment has a superimposed pressure sp, ranging from minimum to maximum as shown above, and with J compartments.

The pressure was varied from the lowest ventilator setting p_{min} = PEEP to the maximum value of p_{max} = PIP (Peek Inspiratory Pressure). Graphs of inflation and deflation can be plotted as shown in Figure 7 from (p_i, V_{inf_i}) and (p_i, V_{def_i}) with $i = 1, 2, \ldots, N$, where N is the size of the vector p.

Bates & Irvin's discrete rate-dependent model

In [6], Bates and Irvin developed a rate-dependent recruitment/derecruitment model based on an alveolus connected to a collapsible airway. If the airway remains open, the alveolar compartment will expand and contract as described by Salazer and Knowles' [33] expression:

$$V = A - Be^{-Kp}, \tag{11}$$

where A, B and K are constants and V is the alveolar compartment volume. If the airway closes, V will remain fixed, i.e. it retains the value it had at the closing pressure until the airway opens, where it will assume the value $V(p)$ from (11). The opening and closing of the airway is governed by $x(t)$ which is given by the following ODE :

$$\frac{dx}{dt} = (p - p_c)\begin{cases}s_{o,} & p > p_c\\ s_{c,} & p < p_c\end{cases},$$

where p_c is a critical pressure which is used alongside x, to determine if the airway is open $(x = 1)$ or closed $(x = 0)$. Note that x is constrained between these values:

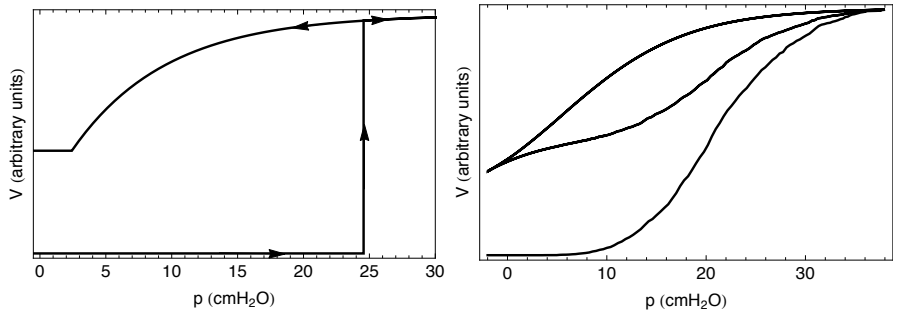

Figure 8: On the left: plot of Bates and Irvin's [6] single aleveolus-airway element. On the right: A plot of the parallel summation of alveolus airway elements, where each element has its own value of p_c, s_o and s_c.

$0 \leqslant x \leqslant 1$. The constants s_o and s_c control the rates at which x approaches opening or closing respectively. A plot of the P-V relationship it generates is shown on the left hand side of Figure 8.

To model the whole lung, they scale the model up by taking a parallel sum of an arbitrary number of these airway-alveolar units, and each unit has its own values of s_o, s_c and p_c, chosen randomly. The probability distribution chosen for p_c was the normal distribution, and s_o, s_c were given a hyperbolic distribution.

6. Preisach model

In the following the Preisach operator will be introduced and some of its properties will be illustrated.

6.1. The hysteron

One of the simplest hysteresis elements, or *hysteron*, is the non-ideal relay. It is characterised by its threshold values $\alpha < \beta$ and internal memory state $\eta(t)$. Its output $y(t)$ can take one of two values 0 or 1: at any moment the relay is either 'switched off' or 'switched on'. The dynamics of the relay are described by the picture in Figure 9.

The variable output $y(t)$

$$y(t) = R_{\alpha,\beta}[t_0, \eta_0]x(t), \qquad t \geqslant t_0, \tag{12}$$

depends on the variable input $x(t)$ $(t \geqslant t_0)$ and on the initial state η_0. Here the input is an arbitrary continuous scalar function; η_0 is either 0 or 1. The scalar function $y(t)$ has at most a finite number of jumps on any finite interval $t_0 \leqslant t \leqslant t_1$. The output behaves rather 'lazily': it prefers to be unchanged, as long as the phase pair $(x(t), y(t))$ belongs to the union of the bold lines in the picture above. The values of function (12) at a moment t are defined by the following explicit formula:

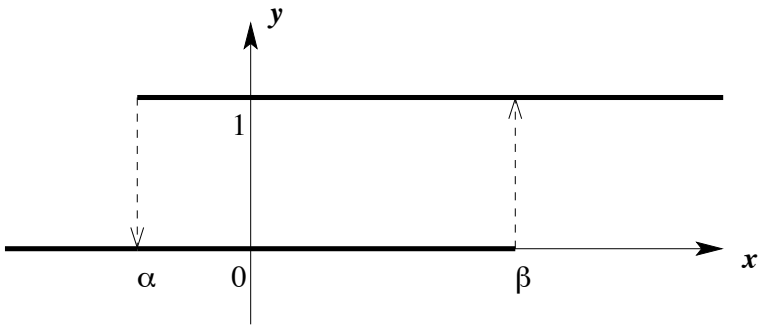

Figure 9: The non-ideal relay.

$$y(t) = R_{\alpha,\beta}[t_0,\eta_0]x(t) = \begin{cases} \eta_0, & \text{if } \alpha < x(\tau) < \beta \text{ for all } \tau \in [t_0,t]; \\ 1, & \text{if there exists } t_1 \in [t_0,t] \text{ such that} \\ & x(t_1) \geqslant \beta,\ x(\tau) > \alpha \text{ for all } \tau \in [t_1,t]; \\ 0, & \text{if there exists } t_1 \in [t_0,t] \text{ such that} \\ & x(t_1) \leqslant \alpha,\ x(\tau) < \beta \text{ for all } \tau \in [t_1,t]. \end{cases}$$

The equalities $y(t) = 1$ for $x(t) \geqslant \beta$ and $y(t) = 0$ for $x(t) \leqslant \alpha$ always hold for $t \geqslant t_0$.

This type of hysteron is one of the most frequently used in hysteresis models as it is the basis of the Preisach model.

6.2. Preisach operators

The main assumption made in the Preisach Model is that the system can be thought of as a parallel summation of a continuum of weighted non-ideal relays $R_{\alpha\beta}$, where the weighting of each relay is $\mu(\alpha,\beta)$. Such a summation can be uniquely represented as a collection of non-ideal relays as points on the two-dimensional half-plane $\Pi = \{(\alpha,\beta) : \beta > \alpha\}$ (see [23]), which is also known as the Preisach plane which is typically shown as in Figure 10. Here the colored area $S = S(t)$ is the set of the threshold values (α,β) for which the corresponding relays $R_{\alpha\beta}$ are in the "on" state at a given moment t. $L(t)$ (the so called staircase) is the interface between the relays, $R_{\alpha\beta}$, which are in the "on" or "off" states. This interface, $L(t)$, evolves according to the rules in section 6.3. The output of the Preisach Model is then represented by the following formula:

$$y(t) = \iint\limits_{\alpha<\beta} \rho(\alpha,\beta) R_{\alpha,\beta}[t_0,\eta_0(\alpha,\beta)]x(t)\, d\alpha d\beta = \iint\limits_{S(t)} \rho(\alpha,\beta)\, d\alpha d\beta. \tag{13}$$

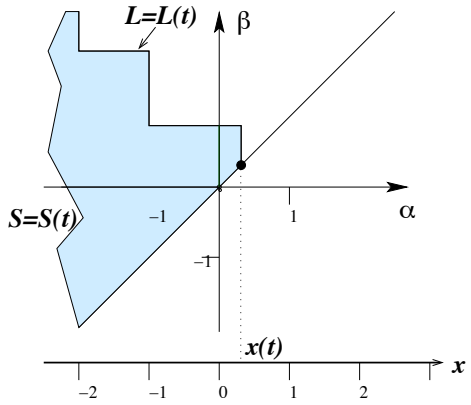

Figure 10: Typical state of a Preisach Plane.

Here $\rho(\alpha,\beta)$ is an integrable positive function in Π. This function is also called *the Preisach density*. We use the following notation to denote the Preisach operator

$$y(t) = (Px)(t).$$

As we see from (13), the output y depends on both the input and the initial values $\eta_0(\alpha,\beta)$ of all relays. Therefore, we sometimes use the more explicit notation

$$y(t) = (P[\eta_0]x)(t).$$

6.3. Geometrical description of the evolution rules

The evolution of the varying "on/off" states admits a simple geometrical interpretation, see Figures 11a and 11b. Here the input $x(t)$, moves along the horizontal scroll-bar, and controls the point on the diagonal $\alpha = \beta$ above itself. When moving toward the upper right corner, this point on the diagonal drags the *horizontal line*, and colors the domain below this line and above the diagonal. For instance, if, in Figure 11a, x increases from the value u to the value v, the colored area is increased by the yellow shaded triangle. When moving towards the bottom left corner in Figure 11b, the diagonal point drags the *vertical line*, and colors yellow everything to the right of this line and above the diagonal. The output $y(t)$ is the area of the blue domain with respect to the measure ρ.

7. Modelling the P-V relationship with the Preisach operator

PROPOSITION 1. *The integral of the Preisach density over any vertical line, $L(h)$ at some point p must equal the derivative $f'(p)$, where $V(p)$ is given by equation*

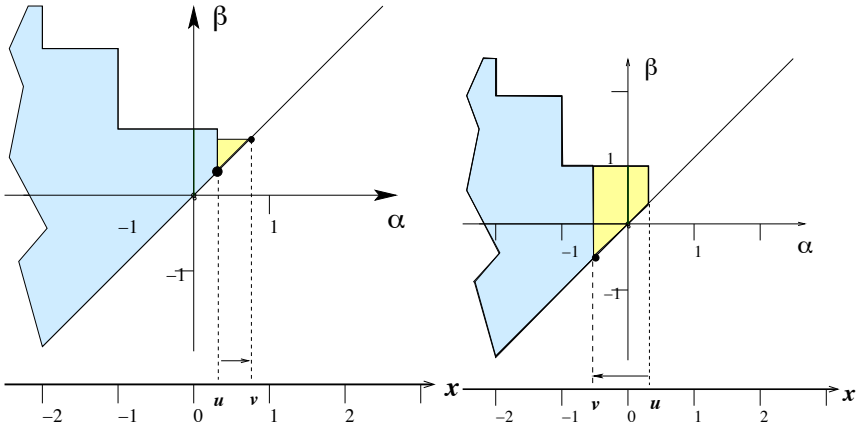

(a) Decreasing input (b) Increasing input

Figure 11: Dynamics of the Preisach Model.

(4) for the main deflation limb i.e.

$$\int_p^{\beta_{max}} \rho(p,\beta)\,d\beta = V'(p). \tag{14}$$

This density is distributed between $\beta = \alpha$ and $\beta = \beta_{max}$, where β_{max} is the maximum β threshold. Moreover, we suggest that the distribution is uniform within the fragment $[p, \beta_{max}]$ of any vertical lines of constant $\alpha \equiv p$. Using Proposition 1 we conclude that this density within this range is given by:

$$\rho(\alpha,\beta) = \frac{V'(\alpha)}{\beta_{max} - \alpha}.$$

We define this density as

$$\rho(\alpha,\beta) \quad = \quad \left(\frac{1}{\beta_{max} - \alpha}\right) \frac{d}{dp}\left(a + \frac{b}{\left(1 + e^{(p-c)/d}\right)}\right), \tag{15}$$

or more succinctly as:

$$\rho(\alpha,\beta) = \frac{b\,\mathrm{sech}^2\left(\frac{c-\alpha}{2d}\right)}{4d(\alpha - \beta_{\max})}. \tag{16}$$

This density is non-zero for $\alpha < \beta < \beta_{max}$, where $0 < \alpha < \beta < \beta_{max}$, and is zero otherwise.

The expression for the inflation curve after the first deflation is given by:

$$V_1(p) = V(p_1) + \int_{\alpha=p_1}^{\alpha=p} \int_{\beta=\alpha}^{\beta=p} \rho(\alpha,\beta)\,d\beta, \tag{17}$$

where p_1 is the pressure at which deflation stops and inflation begins. For convenience let us denote inflation curves with odd subscripts , i.e. by $V_1(p), V_3(p), V_5(p)$ and so on, and deflation curves (other than the main limb) by even subscripts $V_2(p), V_4(p), V_6(p)$ and so on. Since ρ is a function of α only, expression (17) can be reduced to:

$$V_1(p) = V(p_1) + \int_{\alpha=p_1}^{\alpha=p} \frac{b(p-\alpha)\mathrm{sech}^2\left(\frac{c-\alpha}{2d}\right)}{4d\,(\alpha-\beta_{\max})} d\beta. \tag{18}$$

7.1. Results of fitting

The data were extracted by means of specialised software [7] from published experiments. Three datasets were taken from Fig. 6 of Martin et al. [25]. These data, denoted datasets 1 to 3 in Table 2.1 were the measured P-V curves of mice who had lung damage. Dataset 4, was taken from Figure 2a in Koefoed et al. [22] and these data were measure P-V curves pigs lungs that were injured.

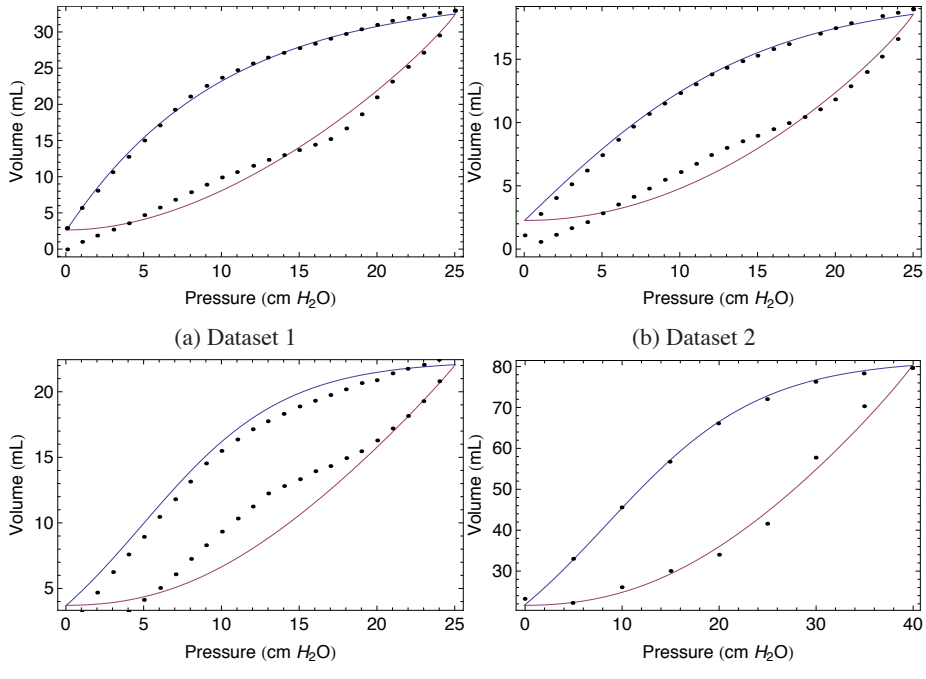

(a) Dataset 1 (b) Dataset 2

(c) Dataset 3 (d) Dataset 4

Figure 12: Results from fitting a Preisach model based on Venegas' equation.

The fitting of the data was done by global minimisation of an objective function

formed from the sum of squared residuals (SSEs):

$$g(a,b,c,d) = \sum_{i=1}^{N} (V(p_i) - V_i)^2 + \sum_{j=1}^{M} (V_1(p_j) - V_{1_j})^2, \tag{19}$$

where g is the objective function and a,b,c and d are the parameters of the model, which are treated like variables for the purposes of optimisation. The constants N and M denote the number of deflation and inflation data points respectively. The global optimisation method used was Differential Evolution [34]. The resulting SSE values and the parameters for each data set are shown in Table 2.1 and the plots are shown in Figure 12. Since the SSE was calculated for datasets whose volumes were not normalised, they cannot be used to compare the results of the fits. Instead an error term was added to Table 2.1 and was calculated as:

$$\frac{\sqrt{SSE}}{V_{max}},$$

where V_{max} is the maximum volume of an individual dataset.

Dataset	Data Source	SSE	Error	a	b	c	d
1	Martin et al. [25]	0.164	0.012	1.02	0.12	2.56	0.18
2	Martin et al.[25]	25.12	0.266	-18.12	38.02	-1.11	-7.91
3	Martin et al. [25]	131	0.502	-2.67	25.03	4.92	-4.56
4	Koefoed et al. [22]	47.1	0.086	0.904	80.87	8.38	-7.96

Table 2.1: Results from fitting P-V curves with the Preisach model.

8. Discussion and Conclusions

In this paper the author focused on several models of P-V relationship of the lungs. Earlier models such expression (2) in section 5.1, captured the P-V curve quite well when the lung was inside the body, where a full sigmoidal curve usually does not occur. This model was also used as the basis of more sophisticated models such as Bates and Irvin's in section 5.2. Later models, such as expressions (3) and (4) in section 5.1 captured the full sigmoidal behaviour, which occurs when the lung is outside the body. It is also possible to fit hysteresis loops with these models, however, the parameters are different for each part of the loop fitted.

Later models attempted to systematically capture the full hysteretic behaviour, these demonstrated that they could qualitatively predict the behaviour of P-V hysteresis loops. The approach in formulating these models is similar to the Preisach model, and further analysis of these may show that they can be reformulated as the Preisach model or a generalised version of it.

Also in this paper, a model was developed based on a similar approach as done for soil hydrology in [12], where a Preisach density was developed based on a function

that fit each branch of the curve successfully. The Preisach model that was developed here had no additional parameters but relied on the parameters of Venegas' function.

The results of the model's fit to the data, can be seen by comparing the error terms in table 2.1. Dataset 1 demonstrated the best fit, followed by datasets 4 and 2. The worst fit was to dataset 3. However, looking at the visual results in Figure 12, dataset 4 shows the best fit qualitatively, followed by datasets 1, 2 and 3.

From looking at Figure 12, it can be seen that the model only captures some of the qualitative behaviour. It does not reproduce the inflection points that can be seen in all the graphs, which is most pronounced in Figure 12c. That indicates that the model needs to be revised further. There are several approaches, firstly the Preisach density can have restrictions placed on it, this will add additional parameters which should improve the fits. Another possibility is to discretely measure the Preisach density using to procedure outlined in Mayergoyz [26]. Additionally the hysteresis models described in this paper may be adapted to develop a new Preisach operator.

The advantage of using hysteresis models such as the Preisach operator models in curve fitting, is that the number of parameters can be substantially reduced. As mentioned above, using earlier models that fit each limb of the hysteresis loop has to be fitted by n parameters, so for k loops you have $n \times k$ parameters in total. Whereas with the Preisach model, the maximum number of parameters required to fit the data would be same n parameters, plus m additional parameters to define the Preisach density. In total $n+m$ parameters could be used to fit any number of hysteresis loops generated from quasi-static P-V measurements. In addition, once the Preisach model has been calibrated it has the ability to predict further loops and thus can be incorporated into differential equations.

References

[1] AMATO M.B., BARBAS C.S., MEDEIROS D.M., SCHETTINO G.D.P., LORENZI FILHO G., KAIRALLA R.A., DEHEINZELIN D., MORAIS C., FERNANDES E.D.O. AND TAKAGAKI T.Y., *Beneficial effects of the "open lung approach" with low distending pressures in acute respiratory distress syndrome. a prospective randomized study on mechanical ventilation*, American Journal of Respiratory and Critical Care Medicine **152** (1995), 1835–1846.

[2] AMATO M.B.P., BARBAS C.S.V., MEDEIROS D.M., MAGALDI R.B., SCHETTINO G.P., LORENZI-FILHO G., KAIRALLA R.A., DEHEINZELIN D., MUNOZ C., OLIVEIRA R., ET AL., *Effect of a protective-ventilation strategy on mortality in the acute respiratory distress syndrome*, New England Journal of Medicine **338** (1998), 347–354.

[3] AMINI R., CREEDEN K. AND NARUSAWA U., *A mechanistic model for quasistatic pulmonary pressure-volume curves for inflation.*, Journal of biomechanical engineering **127** (2005), 619–629.

[4] BACHOFEN H., HILDEBRANDT J. AND BACHOFEN M., *Pressure-volume curves of air- and liquid-filled excised lungs-surface tension in situ.*, Journal of applied physiology **29** (1970), 422–431.

[5] BATES J.H., *Lung mechanics: an inverse modeling approach*, Cambridge University Press, Cambridge 2009.

[6] BATES J.H. AND IRVIN C.G., *Time dependence of recruitment and derecruitment in the lung: a theoretical model*, Journal of Applied Physiology **93** (2002), 705–713.

[7] BORMANN I. *Digitizeit version 1.5. 8b*, 2010.

[8] CARVALHO A. AND ZIN W., *Respiratory mechanics: Principles, utility and advances*, In *Anaesthesia, Pharmacology, Intensive Care and Emergency Medicine APICE*, Springer, Milan 2011, 33–46.

[9] CHASE J.G., YUTA T., MULLIGAN K.J., SHAW G.M. AND HORN B., *A novel mechanical lung model of pulmonary diseases to assist with teaching and training*, BMC pulmonary medicine **6** 21 (2006) 1–11.

[10] CHENG W., DELONG D., FRANZ G., PETSONK E. AND FRAZER D., *Contribution of opening and closing of lung units to lung hysteresis*, Respiration physiology **102** (1995), 205–215.

[11] CLOETTA M., *Untersuchungen über die elastizität der lunge und deren bedeutung für die zirkulation*, Pflüger's Archiv für die gesamte Physiologie des Menschen und der Tiere **152** (1913), 339–364.

[12] FLYNN D., MCNAMARA H., O'KANE P. AND POKROVSKII A., *Application of the Preisach model to Soil-Moisture Hysteresis*, Science of Hysteresis, vol. 3, Academic Press, Oxford 2005, (689–744).

[13] GANZERT S., KRAMER S. AND GUTTMANN J., *Predicting the lung compliance of mechanically ventilated patients via statistical modeling*, Physiological Measurement **33** (2012), 345–359.

[14] GREAVES I.A., HILDEBRANDT J. AND HOPPIN F.G., *Micromechanics of the lung*, Comprehensive Physiology (2011), 217–231

[15] HARRIS R.S., *Pressure-volume curves of the respiratory system*, Respiratory care **50** (2005), 78–99.

[16] HEROLD R., DEWITZ R., SCHÜRCH S. AND PISON U., *Pulmonary surfactant and biophysical function*, Studies in Interface Science **6** (1998), 433–474.

[17] HICKLING K.G., *The pressure–volume curve is greatly modified by recruitment: a mathematical model of ARDS lungs*, American journal of respiratory and critical care medicine **158** (1998), 194–202.

[18] HILDEBRANDT J., *Pressure-volume data of cat lung interpreted by a plastoelastic, linear viscoelastic model*, Journal of applied physiology **28** (1970), 365–372.

[19] HILLS B., *Contact-angle hysteresis induced by pulmonary surfactants*, Journal of Applied Physiology **54** (1983), 420–426.

[20] HUTCHINSON J. AND TODD R.B., *Cyclopedia of anatomy and physiology*, Thorax **4** (1849), 1016–1087.

[21] JONSON B. AND SVANTESSON C., *Elastic pressure–volume curves: what information do they convey?*, Thorax **54** (1999), 82–87.

[22] KOEFOED-NIELSEN J., ANDERSEN G., BARKLIN A., BACH A., LUNDE S., TØNNESEN E. AND LARSSON, A., *Maximal hysteresis: a new method to set positive end-expiratory pressure in acute lung injury?*, Acta Anaesthesiologica Scandinavica **52** (2008), 641–649.

[23] KRASNOSELSKII M.A. AND POKROVSKII A., *Systems with hysteresis*, Springer-Verlag, Berlin 1989.

[24] LIGAS J.R., *Lung tissue mechanics: Historical overview*, Respiratory Biomechanics, Springer, New York 1990, (3–18).

[25] MARTIN E.L., MCCAIG L.A., MOYER B.Z., PAPE M.C., LECO K.J., LEWIS J.F. AND VELDHUIZEN R.A., *Differential response of timp-3 null mice to the lung insults of sepsis, mechanical ventilation, and hyperoxia*, American Journal of Physiology-Lung Cellular and Molecular Physiology **289** (2005), 244–251.

[26] MAYERGOYZ I.D., *Mathematical models of hysteresis and their applications*, Academic Press, 2003.

[27] MEAD J., *Mechanical properties of lungs*, Physiological Reviews **41** (1961), 281–330.

[28] MILIC-EMILI J. AND D'ANGELO E., *Statics of the lung*, Physiologic basis of respiratory disease, BC Decker Incorporated 2005, (27–33).

[29] MOLS G., PRIEBE H.J. AND GUTTMANN J., *Alveolar recruitment in acute lung injury*, British journal of anaesthesia **96** (2006), 156–166.

[30] MURPHY B. AND ENGEL L., *Models of the pressure-volume relationship of the human lung*, Respiration physiology **32** (1978), 183–194.

[31] PETTY T.L., *The use, abuse, and mystique of positive end-expiratory pressure*, The American review of respiratory disease **138** (1988), 475–478.

[32] ROZANEK M. AND ROUBIK K., *Mathematical model of the respiratory system–comparison of the total lung impedance in the adult and neonatal lung*, Proceedings of the World Academy of Science, Engineering and Technology **24** (2007), 293–296.

[33] SALAZAR E. AND KNOWLES J.H., *An analysis of pressure-volume characteristics of the lungs*, Journal of Applied Physiology **19** (1964), 97–104.

[34] STORN R. AND PRICE K., *Differential evolution–a simple and efficient heuristic for global optimization over continuous spaces*, Journal of global optimization **11** (1997), 341–359.

[35] SUKI B., ANDRADE JR J.S., COUGHLIN M.F., STAMENOVIĆ D., STANLEY H.E., SUJEER M. AND ZAPPERI S., *Mathematical modeling of the first inflation of degassed lungs*, Annals of biomedical engineering **26** (1998), 608–617.

[36] SUKI B., BARABASI A.L., HANTOS Z., PETÁK F. AND STANLEY H.E., *Avalanches and power-law behaviour in lung inflation*, Nature **368** (1994), 615–618.

[37] SUKI B. AND BATES J.H., *Lung tissue mechanics as an emergent phenomenon*, Journal of Applied Physiology **110** (2011), 1111–1118.

[38] VON NEERGAARD K., *Neue auffassungen über einen grundbegriff der atemmechanik*, Research in Experimental Medicine **66** (1929), 373–394.

[39] VENEGAS J.G., HARRIS R.S. AND SIMON B.A., *A comprehensive equation for the pulmonary pressure-volume curve*, Journal of Applied Physiology **84** (1998), 389–395.

[40] WARE L.B. AND MATTHAY M.A., *The acute respiratory distress syndrome*, New England Journal of Medicine **342** (2000), 1334–1349.

AMS Subject Classification: 92C35, 76Z05, 92C50, 47J40

Denis FLYNN,
Centre of Excellence Telč
Batelovska 485, 486
588 56 Telč,
CZECH REPUBLIC
e-mail:flynn@itam.cas.cz

Lavoro pervenuto in redazione il 29.01.2015.